Screening Gas-Phase Chemical Kinetic Models: Collision Limit Compliance and Ultra-Fast Time Scales

Kiran K. Yalamanchi[1*], Efstathios-Al. Tingas[1,2*], Hong G. Im[1],
S. Mani Sarathy[1*]

[1]King Abdullah University of Science and Technology (KAUST), Clean Combustion Research Center, Physical Sciences and Engineering Division, Thuwal, Saudi Arabia
[2]Perth College, University of the Highlands and Islands (UHI), Crieff Rd, Perth, PH1 2NX, UK
*corresponding author email: kiran.yalamanchi@kaust.edu.sa; stathis.tingas@kaust.edu.sa; mani.sarathy@kaust.edu.sa

Abstract

Detailed gas-phase chemical kinetic models are widely used in combustion research and many new mechanisms for different fuels and reacting conditions are developed each year. Recent works have highlighted the need for error checking when preparing such models, but a useful community tool to perform such analysis is missing. In this work, we present a simple online tool to screen chemical kinetic mechanisms for bimolecular reactions exceeding collision limits. The tool is implemented on a user-friendly website, cloudflame.kaust.edu.sa, and checks three different classes of bimolecular reactions; (i.e., pressure independent, pressure dependent falloff, and pressure dependent PLOG). In addition, two other online modules are provided to check thermodynamic properties and transport parameters to help kinetic model developers determine the sources of errors for reactions that are not collision limit compliant (CLC). Furthermore, issues related to unphysically fast time scales can remain an issue even if all bimolecular reactions are within collision limits. Therefore, we also present a procedure to screen ultra-fast reaction time scales using computational singular perturbation (CSP). For demonstration purposes only, three versions of the rigorously developed AramcoMech are screened for collision limit compliance and ultra-fast time scales, and recommendations are made for improving the models. Larger models for biodiesel surrogates, tetrahydropyran, and gasoline surrogates are also analysed for exemplary purposes. Numerical simulations with updated kinetic parameters are presented to show improvements in wall-clock time when resolving ultra-fast time scales.

1. Introduction

Chemical kinetic models are widely used to simulate fuel oxidation and pyrolysis during combustion. With the increasing demand for reliable kinetic models, the number of mechanisms being published has increased in recent time.[1,2] Many recent models are widely validated against global combustion properties and species measurements in shock tubes and rapid compression machines, premixed and non-premixed flames, perfectly stirred reactors, and flow reactors. Despite such comprehensive validations, the sheer size of these mechanisms and their hierarchical nature often results in error propagation in kinetic and thermodynamic parameters that is difficult to identify and correct.

With the availability of high computational power and need to predict the behaviour of realistic complex fuels, the typical mechanism size has recently increased significantly. For example, a gasoline toluene-PRF surrogate mechanism by Mehl et al.[3] is composed of over 1500 species and 6000 reactions. Since calculating rates for such a large number of reactions accurately is an expensive task, they are often determined by making some approximations and assumptions similar to the rate rules by Sarathy et al.[4] All of the individual species must also be accompanied with thermodynamic properties, often calculated using group additivity rules[5], and transport properties generated with certain correlations[6].

Following theories by van't Hoff and Arrhenius as the basis for systematic description of chemical reactions[7,8], today's gas-phase chemical kinetic mechanisms consist of many elementary reactions in the form of Arrhenius equations for detailing the specific nature of reaction processes. In reacting systems, the Smoluchowski diffusion limit can be used to estimate bimolecular rate constants without needing any molecular information regarding the reacting species; it is dependent only on the properties of the solvent (viscosity) and temperature. In combustion systems, collision theory[9] for gas-phase bimolecular reactions sets the upper limit on rate coefficient, referred to as the collision limit. For complex kinetic mechanisms, however, many rate constants are inevitably built up by curve-fitting based on a finite number of data points, and are subject to errors that may exceed the collision limit. Chen et al.[10] examined a number of recently published kinetic mechanisms and reported that a large number of reaction rates exceed the collision limit, and further suggested the need for a computational tool for researchers to conduct the rate coefficient screening for collision limit compliance (CLC).

In addition to bimolecular gas-phase reactions exceeding collision limits, other types of reactions (e.g., unimolecular decomposition, isomerization, etc.) may exceed physically reasonable timescales. Chemical reactions typically evolve in a wide range of timescales, some of them being extremely fast. According to Zewail[11], "*the speed of atomic motion is about 1 km/s and, hence, to record atomic-scale dynamics over a distance of an angström, the average time required is approximately 100 fs*". Therefore, gas-phase chemical reactions with time scales in the range of 1 ps and 1 fs are unlikely, and reactions faster than 1 fs are considered unphysical. Unfortunately, such time scales are frequently encountered in existing chemical kinetic models used in combustion simulations, as shown herein. Note, also, that there are often situations in multi-dimensional turbulent combustion problems, in which turbulent transport may lead to local thermodynamic conditions well outside the usual conditions explored in idealized reduced-dimensional configurations used in the kinetic model development. This results in large numerical *stiffness*, implying that the fastest chemical time scales are many orders of magnitude smaller than the time scales to describe the system dynamics such as ignition and flame propagation. Kinetic mechanisms exhibiting such ultra-fast time scales lead to non-physical predictions as well as a significant computational burden for large scale simulations.

For the practitioners implementing such mechanisms in reacting flow simulations, the computational burden is commonly alleviated by splitting the chemical reaction source terms from the convective and diffusive transport operators, and employing an implicit time integration for the stiff reaction terms. However, such an approach comes at its own overhead as the implicit method requires a computation of the large Jacobian matrix and iterative solution

techniques. Furthermore, the numerical errors associated with the operator splitting must also be carefully accounted for. Alternatively, one may argue that such ultra-fast chemical time scales that relate to non-physical rate constants should not exist in the first place, so that a properly developed kinetic mechanism should be amenable to explicit time integration schemes which are computationally simple and inexpensive. In direct numerical simulations (DNS) where the smallest turbulent eddies and flame structures are fully resolved, the minimum time scales required by the turbulent flame dynamics may approach on the order of nanoseconds, which may not be far off from the relevant and physically valid fast chemical time scales.

The present study attempts to provide insights into the aforementioned issues in order to guide future development of kinetic mechanisms that are physically sound and computationally efficient. Collision limit violations are identified for bimolecular reactions, and ultra-fast times scales in both unimolecular and bimolecular reaction resulting in chemical stiffness are identified. First, a number of published kinetic mechanisms are examined to identify whether the chemical time scales exceed the collision limits, and if so, under what conditions they are encountered. The selection of models is not intended to be comprehensive nor is it meant to place judgement on the model developers. A systematic tool for an initial screening of the fast chemical time scales is developed for public use under the KAUST CloudFlame[12], a website that provides a front-end for data search tools and web-based numerical simulations. The CLC tool requires transport data for all species in the mechanism, which is sometimes not available in large detailed kinetic models. Second, the evolution of fast time scales in a dynamic system is also analysed by use of the computational singular perturbation (CSP) framework[13,14], which is an automated asymptotic analysis to identify the critical time scales from a complex multi-scale phenomena. The CSP framework has successfully been used to develop reduced and simplified kinetics model[15-19], to diagnose the key species and processes[20-25] and to characterize the flame topology.[26,27] In the present study, the time scale participation index (TPI) is mainly used to identify the reactions related to the fast time scales.[28-32]

In the following, the details of the CLC analysis and CSP approach are described. Violations to the collision limit are then investigated with modules for determining the source of errors, using the AramcoMech series of kinetic models as a test case. We reiterate that these were chosen only for exemplary purposes and not intended to base judgement on the models or their developers. This is followed by a more detailed analysis of ultra-fast time scales in various kinetic models available in the literature. Note that the present test results are based on conservative criteria for the extremely fast chemical time scales only. As such, the results must be taken as an exemplary demonstration to provide a better understanding of the general causes for the fast time scales, and the result is not intended to be the final mechanisms, for which further refinements and validations are needed.

2. Methodology

2.1 Collision Limit Compliance

At any given temperature, the number of collisions happening per unit time sets an upper limit on the gas phase bimolecular reaction rate. For the detailed kinetic mechanisms under consideration, the chemical time scale for each bimolecular reaction was evaluated and checked if it is within the physical limit. The CLC tool utilizes the Cantera suite of codes[33] for processing the kinetic model and calculating thermodynamic, transport and rate information. The mechanism file is provided in .cti format, and a user can specify a fixed temperature or range of temperatures at which the model is tested for CLC. The tool is available via a web interface at https://cloudflame.kaust.edu.sa/violation_check. The code is also available on the following Githhub repository (https://github.com/kiranyalamanchi/CLC_script). The output generated is self-explanatory, with all the values in SI units. Additionally, the 'Mechanism File Converter' tool (https://cloudflame.kaust.edu.sa/ck2cti/converter) on CloudFlame converts a mechanism from Chemkin format to Cantera (.cti) format, if required.

The tool checks CLC for three different classes of bimolecular reactions, i.e., pressure independent, pressure dependent fall-off (TROE or SRI), and pressure dependent PLOG. For all of these classes, the collision limit is calculated using the formula:

$$k_{col} = \sqrt{\frac{8\pi k_B T}{\mu}}\ \sigma^2 \Omega^{(1,1)^*} N_a$$

where T is temperature, k_B is the Boltzmann constant, μ is reduced mass, σ is the collision diameter of the Lennard–Jones (LJ) 12-6 potential and N_a is the Avogadro number, and $\Omega^{(1,1)^*}$ is the reduced collision integral[34]. For reactions without pressure dependence, the rate coefficient is compared to the collision limit, and the rate coefficient is calculated by

$$k_{fi} = A \cdot T^b \cdot e^{-\frac{E_a}{RT}}$$

where A, b and E_a are the Arrhenius coefficients provided in the chemical kinetic mechanism, T is the temperature and R is the gas constant. For fall-off reactions in the TROE and SRI formalism, the rate at a specific temperature and pressure depends on the high-pressure limit, low-pressure limit, third body efficiencies, and concentrations of other species. Further details on fall-off reaction rate formulation can be found from Cantera documentation[33]. For these reactions, only the high-pressure limit, the fastest case, is compared against the collision limit. For PLOG reactions, the rate coefficients are provided at discrete pressures, and the rate constant at any other pressure is interpolated from these values. As such, the rate coefficient at each pressure designated in the mechanism file is compared against the collision limit. For a reversible reaction, the reverse rate constant is calculated based on the equilibrium constant K_{Cj} and k_{fj}, equal to $k_{rj} = \frac{k_{fj}}{K_{Cj}}$. Therefore, a high k_{fj} and low K_{Cj} can compound to cause the reverse rate to exceed the collision limit. Note that the rate parameters for most of the reactions in kinetic mechanisms are fitted parameters, and are fitted to provide the rate coefficient of the reaction at various temperatures with other details being left out. For example, E_a may not represent activation energy for every reaction. Therefore, the kinetic mechanisms

are screened only for the overall rate coefficients of reactions and not on individual rate parameters.

Reaction mechanisms typically define parameters in a single direction, and the reverse rate of reaction is determined from thermochemistry. The CLC tool compares both forward and reverse rates against their respective collision limit and reports the results. When the input is a single temperature, the final downloadable output provides all reactions exceeding the collision limit alongside their rate coefficient and respective calculated collision limit. For PLOG reactions, all the rate coefficients that exceed the collision limit are reported, along with the pressure values. For all reverse reactions exceeding collision limits, the forward reaction rate coefficient and equilibrium constants are reported as well. In case of a parametric temperature input, the first part of the output file displays all reactions exceeding the collision limit in the prescribed temperature range, and the temperatures at which each of these reactions rate coefficients are unphysical. The second part of the output file is similar to the single temperature output file for every temperature value parameterized. For illustration, output files are provided in the Supplementary Material, for the published mechanisms used.

Note that CLC violations may arise in several cases and from various parameters, i.e., forward rate coefficient, equilibrium constant, or the calculated collision limit. Following is a list of some cases that lead to a reaction rate coefficient violating collision limits:

1. Forward reaction rate is correctly determined but the reverse rate may exceed collision limit due to discrepancies in ΔH and ΔS of the reaction. If the reaction is elementary and A-factor and E_a are not fitted parameters, then ΔH and ΔS of the reaction affects E_a and A-factor of reverse reaction, respectively.
2. Rate parameters are derived by fitting to either experimental data or computed rate coefficients, in which data are limited to a narrow temperature range. Outside the tested temperature range, the fit may sometimes result in unphysical values. In addition, using an incorrect fitting function (e.g., three parameter Arrhenius) for reactions that do not show strong Arrhenius dependence or reactions that require more parameters to fit accurately.
3. Extension of rate parameters with respect to pressure based on data at a limited number of pressure conditions. A small error can lead to an unphysical high-pressure limit or an erroneous value at low pressures.

While the forward rate coefficient depends on the parameters prescribed in the mechanism file, the equilibrium constant and collision limit depend on thermodynamic and transport parameters, respectively. Since uncertainties in rate coefficients are generally higher than thermodynamic and transport parameters, rate parameters are usually the most probable cause of violations. Nevertheless, it is necessary to check thermodynamic and transport parameters of species involved in a reaction, as errors in these may also cause the CLC violations. To summarize, if a forward rate coefficient exceeds the collision limit, rate and transport parameters are checked; if a reverse rate coefficient exceeds the collision limit, thermodynamic parameters are also checked along with rate and transport parameters.

Correcting the rate parameters requires checking the original source of the parameters and conducting a more detailed analysis on fittings, estimates, etc. To help users determine if CLC violations are due to transport or thermodynamic data, two additional modules are provided. The transport parameter calculator provides the value for the collision diameter and well depth when the boiling temperature, critical temperature, and pressure of a molecule are given as inputs. These parameters are calculated using correlations by Tee et al.[6], and the values help the user to cross-validate the transport data of species involved in reactions exceeding collision limits. The second module is the thermodynamics property checker which, for a mechanism file and a violating reaction number provided in the CLC output file, reports the valid temperature range for the NASA polynomial of the species, along with plots of heat capacity, enthalpy and entropy with respect to temperatures. This information is provided for all the species in the violating reaction. Any anomaly in the plots of heat capacity, enthalpy and entropy indicates that the thermodynamic parameters require more scrutiny. It should be noted that chemical kinetics reaction mechanisms may contain lumped reactions that are a combination of elementary reactions. In such cases, it is hard to identify the collision limit for the various elementary steps, since that information is not available in the reaction mechanism. In this work, the lumped reactions that are found to exceed collision limits need to be revisited, since the total lumped reaction rate should be less than that of the sum of elementary reactions with the same reactants, which is bounded by collision limit.

2.2 Computational Singular Perturbation

For dynamical analysis of the chemical system, CSP is used to identify reactions in chemical kinetic model that generate ultra-fast times scales during a reacting flow simulation. In the case of the batch reactor (constant volume or pressure), the system of species and energy governing equations is cast in the general form:

$$\frac{d\boldsymbol{z}}{dt} = \boldsymbol{g}(\boldsymbol{z}) = \widehat{\boldsymbol{S}}_1 \cdot R^1 + \cdots + \widehat{\boldsymbol{S}}_{2K} \cdot R^{2K} \quad (1)$$

where $\boldsymbol{z}$ is the vector including the *N*-species mass fractions and temperature ($\boldsymbol{z} = [\boldsymbol{y}, T]^T$), $\boldsymbol{g}(\boldsymbol{z})$ is the chemical source term, $\widehat{\boldsymbol{S}}_i$ is the generalized stoichiometric vector of the *i*-th reaction, R^i the respective reaction rate and *2K* is the total number of unidirectional reactions. Note that $\widehat{\boldsymbol{S}}_i$ is an *(N+1)*-dimensional column vector with its top *N* elements being functions of the system's stoichiometric coefficients, the species' molecular weights and density, while its last element (that relates to temperature) adds a functional dependence on the species' absolute enthalpies, the mixture's heat capacity and temperature. Based on the CSP approach, Eq. 1 is rewritten in terms of the CSP basis vectors $\boldsymbol{a}_i$ and their related amplitudes $f^i = \boldsymbol{b}^i \cdot \boldsymbol{g}(\boldsymbol{z})$, $b^i \cdot a_j = \delta_j^i$ [14,15]:

$$\frac{d\boldsymbol{z}}{dt} = \boldsymbol{g}(\boldsymbol{z}) = \boldsymbol{a}_1 f^1 + \boldsymbol{a}_2 f^2 + \cdots \boldsymbol{a}_N f^N + \boldsymbol{a}_{N+1} f^{N+1} \quad (2)$$

The CSP basis vectors $\boldsymbol{a}_i$ and $\boldsymbol{b}^i$ are calculated through two iterative procedures[14,35-37], but in the current work they have been approximated by their leading order approximations, i.e., the right and left eigenvectors of the Jacobian ($\boldsymbol{J}$) of $\boldsymbol{g}(\boldsymbol{z})$[38-40], which is a common practice when interested in identifying the key process in reacting systems.[15-32] Each CSP mode is described

by an amplitude f^i, which signifies the impact of that mode to the system's slow evolution, and a timescale τ_i, which sets the timeframe of action of the mode, is approximated by the inverse norm of the related eigenvalue, i.e., $\tau_i = \frac{1}{|\lambda_i|}$, $\lambda_i = \boldsymbol{b}^i \cdot \boldsymbol{J} \cdot \boldsymbol{a}_i$.[13,14] Since $\boldsymbol{J} = \boldsymbol{\nabla}(\widehat{\boldsymbol{S}}_1 R^1) + \cdots + \boldsymbol{\nabla}(\widehat{\boldsymbol{S}}_{2K} R^{2K})$, each system's *i*-th eigenvalue can be expressed as:

$$\lambda_i = \boldsymbol{b}^i \cdot \boldsymbol{\nabla}(\widehat{\boldsymbol{S}}_1 R^1) \cdot \boldsymbol{a}_i + \cdots + \boldsymbol{b}^i \cdot \boldsymbol{\nabla}(\widehat{\boldsymbol{S}}_{2K} R^{2K}) \cdot \boldsymbol{a}_i \quad (3)$$

which implies that each eigenvalue is the weighted sum of the reaction rate gradients against the species mass fractions and temperature.

Based on Eq. 3, the timescale participation index (TPI) is introduced, measuring the contribution of the *k*-th reaction to the system's *i*-th timescale[38,39]:

$$TPI_k^i = \frac{\boldsymbol{b}^i \cdot \boldsymbol{\nabla}(\widehat{\boldsymbol{S}}_k R^k) \cdot \boldsymbol{a}_i}{\left|\boldsymbol{b}^i \cdot \boldsymbol{\nabla}(\widehat{\boldsymbol{S}}_1 R^1) \cdot \boldsymbol{a}_i\right| + \cdots + \left|\boldsymbol{b}^i \cdot \boldsymbol{\nabla}(\widehat{\boldsymbol{S}}_{2K} R^{2K}) \cdot \boldsymbol{a}_i\right|}$$

where $i = 1, \ldots, N+1$, $k = 1, \ldots, 2K$ and by definition $\sum_{k=1}^{2K} |TPI_k^i| = 1$. The TPI tool has been used extensively in the field of reacting flows in many different configurations mainly for the purpose of identifying the chemical reactions related to the system's explosive timescale.[19-25,27-32,38-43] In the current analysis, the TPI tool is employed to identify the reactions that generate the ultra-fast timescales.

For the *i*-th unimolecular and unidirectional reaction (forward or reverse), where only one reactant is included and its rate constant k_{fi} or k_{ri} (forward and reverse, respectively) is calculated based on the Arrhenius equation, the elements in the $\boldsymbol{\nabla}(\widehat{\boldsymbol{S}}_i R^i)$ matrix have minimum absolute value of zero and maximum k_{fi} *or* k_{ri}. For the *j*-th reverse unimolecular reaction where only one reactant is included and its rate constant is calculated based on the equilibrium constant K_{Cj} and k_{fj}, the elements of the $\boldsymbol{\nabla}(\widehat{\boldsymbol{S}}_j R^j)$ matrix will have minimum absolute value of zero and maximum equal to $k_{rj} = \frac{k_{fj}}{K_{Cj}}$, so it will be a function of the Arrhenius coefficients of the forward and the species thermodynamic properties.

According to Eq. 3, each eigenvalue is the result of the weighted sum of the gradients of the reaction rates against the species mass fractions and temperature. Therefore, unless a reaction includes one reactant (such as in unidirectional and unimolecular dissociation/isomerization reactions), these gradients may differ significantly from the respective rate constants. In addition, a reaction with a large rate constant may be weakly related to a fast direction of the subspace spanned by the CSP basis vectors, i.e., the related component in the basis vectors is negligibly small, and thus the contribution of that reaction to the fast eigenvalue is small. In other words, a reaction with a very large rate constant may not produce a very large eigenvalue either because the related gradients are small or because of its small weight. Nonetheless, unidirectional and unimolecular dissociation/isomerization reactions with large rate constants are most likely to relate to ultra-fast timescales. In such a case, if the Arrhenius coefficients are explicitly provided in the mechanism, the revision of the coefficients is straightforward. If not (e.g., in the event of a reverse reaction that no Arrhenius coefficients are explicitly provided in the mechanism), the revision of the related reaction rate constant is complicated since it is a

function of many variables as discussed in previous subsection, and is more difficult to correct. It is noted in the context of the current work, as "ultra-fast" are characterized as time scales faster than one 1 fs.

3. Results and Discussion

3.1 Screening models for CLC

The CLC tool was used to screen three versions of AramcoMech (i.e., 1.3[44], 2.0[45,46] and 3.0[47]) and the Foundational Fuel Chemistry Model Version 1.0 (FFCM-1)[48] for reaction rates exceeding collision limits. These models were selected because they contain transport data for all species in the reaction mechanism, and the models have been rigorously developed. It should be noted that models developed by authors at KAUST[49-51] also exhibited CLC violations, but were not selected in the examples presented here because KAUST models often do not provide transport data for all species (e.g., low temperature radical species ROO, QOOH, etc.). A temperature range of 300 – 2000 K in increments of 50 K was chosen for screening, which is relevant for combustion simulations. A list of violating reactions in AramcoMech 1.3 are detailed in Table 1. Details of CLC violations in AramcoMech 2.0 and 3.0 and FFCM-1 can be found in the Supplementary Material. All models were found to exhibit one or more CLC violations. We found that some reaction rates in AramcoMech 1.3 that violated collisions limits were updated and corrected in AramcoMech 2.0 and 3.0, as discussed below. Therefore, improvements to chemical kinetic models by scrutinizing rate parameters helps to meet CLC. However, it was also found that several new reactions added in recent models exceed collision limits, which requires a recheck of collision limits when any new reactions added. For reactions 1-5 in Table 1, CLC violations were found for the forward pressure independent rate parameters, while for reactions and 7-10, violations were found for the reverse pressure independent rate parameters. Reactions 6 and 11 are both pressure dependent falloff reactions for which the forward and reverse rate coefficients, respectively, exceeded collision limits. All the PLOG reaction rates in AramcoMech 1.3 were found to be within collision limits.

Table 1 – List of reactions and corresponding temperature range in which CLC violations were identified for AramcoMech 1.3. Reactions were only screened at temperatures between 300 K and 2000 K.

Rxn. No	Reaction	Temperature range (K)
	Forward	
1	H2O + OH* => H2O + O	300 - 2000
2	OH + OH* => 2 OH	300 - 2000
3	CO2 + OH* => CO2 + OH	300 - 400
4	CO + OH* => CO + OH	300 - 400
5	CH + CH2O => CH2CO + H	300
6*	C2H + H (+M) => C2H2 (+M)	300 - 2000
	Reverse	
7	2 C2H4 <= C2H3 + C2H5	300
8	O2C2H4OH <= O2 + PC2H4OH	300 - 400

9	HO2CH2OCHO <= OCH2OCHO + OH	300 - 2000
10	NC3H7O2H <= NC3H7O + OH	300 - 2000
11*	CH3OH (+M) <= CH2OH + H (+M)	300 - 500

* - collision limit calculated at high pressure limit

To demonstrate the utility of our CLC tool and supporting scripts, we further investigated the reactions presented in Table 1 and the source of errors. Reactions 1-4 are included in mechanism to simulate chemiluminescence of OH*; this sub-mechanism is derived from the work of Kathrotia et al.[52] The rates for reactions 1-4 were originally obtained from Tamura et al.[53] on collisional quenching in low pressure flames, which determined quenching rate coefficients for OH* with various collider species (e.g., CO_2, H_2O, CO). They noted that quenching rates provided are for the $\nu=0$ level of the electronically excited OH* and that higher vibrational levels are not considered. Due to these uncertainties, and the fact that chemiluminescence reactions contribute little to the main combustion chemistry pathways[52], we did not attempt to resolve non-compliance in chemiluminescence reactions.

All the other rates in Table 1 were changed to comply with their collision limits. Reactions 5 and 7 exceed collision limits at low temperatures of 300 K; therefore, the Arrhenius fitting parameters were modified to constrain the rate at 300 K to the collision limit value while maintaining the same rate at other temperatures. Reaction 6 has pressure dependent parameters in the TROE formalism, for which the high pressure limit exceeds the collision limit. To resolve this discrepancy, the high pressure limit was changed to that provided by Harding et al.[54], which does not exceed collision limit. We found that the thermodynamic data of species in reactions 8, 9 and 10, except O_2 and OH, were updated in later versions of AramcoMech. Incorporating these changes into AramcoMech 1.3 made these reactions collision limit compliant. For reaction 11, the high pressure limit Arrhenius parameters were modified to fit within the collision limit from 300-500 K, while keeping the same rate at other temperatures. The modified AramcoMech 1.3 mechanism with the aforementioned modifications is provided as Supplementary Material.

3.2 Screening models for ultra-fast timescale analysis of AramcoMech

3.2.1 The AramcoMech 2.0 kinetics mechanism

Next, AramcoMech 2.0 was selected for an extensive timescale analysis, for a number of reasons. First, it was validated against a wide range of operating conditions, and is widely used in the combustion community. Secondly, it includes chemistry from C1 up to C4, offering the opportunity to assess the response of the ultra-fast timescales to different mixture compositions. Finally, it is a mechanism of medium size (493 species and 2716 reversible reactions); small enough for the computationally expensive analysis and sufficiently large for the development of ultra-fast timescales, which usually emerge in mechanisms of medium to large sizes.

The analysis was performed on the basis of a batch reactor model (constant volume) in a wide range of initial conditions in the parametric space ($0.1 < \varphi < 6.0,\ 600K < T(0) < 2200K,\ 0.6atm < p(0) < 100atm$), and the following fuels were tested, in a total of more than 400 different sets of initial conditions: CH_4, C_2H_6, C_3H_8, C_2H_4, C_2H_2, C_2H_5OH, C_3H_6, CH_2O, CH_3CHO, CH_3COCH_3, CH_3OH, CH_3OCH_3, iC_4H_{10}, iC_4H_8. Both the generation of the batch reactor solution and the analysis were performed using CSPTk[55], a software employing the TChem package[56] for the thermo-kinetic database management. Considering the large dynamic range of the system's eigenvalues, results will be shown in logarithmic scale as follows:

$$\Lambda_i = sign(\lambda_i) \cdot log_{10}|\lambda_i|$$

In the following, only 3 cases will be analyzed and reported in detail, but their results are representative of the findings identified in all studied cases. Figure 1 displays with red and black colors the evolution of the system's temperature and the ten fastest eigenvalues, respectively, for three different mixture compositions, representative of the low, intermediate and high temperature regimes:

- CH_3OCH_3/air, $p(0) = 25.7\ atm,\ T(0) = 600\ K,\ \varphi = 2.0$
- iC_4H_8/air, $p(0) = 30.0\ atm,\ T(0) = 1{,}100\ K,\ \varphi = 1.0$
- CH_4/air, $p(0) = 4.1\ atm,\ T(0) = 1{,}724\ K,\ \varphi = 0.1$

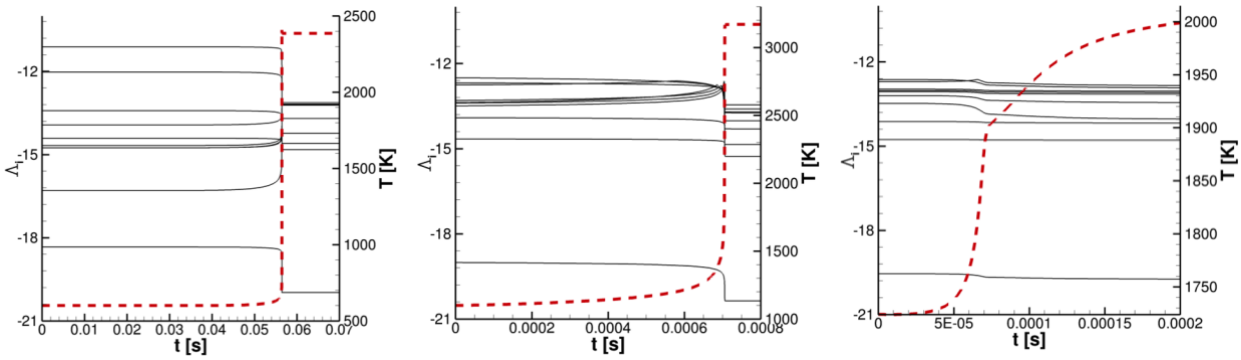

Figure 1: The evolution of temperature and the developing ten smallest eigenvalues with red-dashed and black-solid lines, respectively, for CH_3OCH_3/air (p(0)=25.7 atm, T(0)=600 K, φ=2.0) on the left, iC_4H_8/air (p(0)=30.0 atm, T(0)=1,100 K, φ=1.0) in the middle and CH_4/air (p(0)=4.1 atm, T(0)=1,724 K, φ=0.1) on the right.

It is shown that, in terms of fast timescales, the intermediate and high temperature cases look similar, i.e. in both cases only one eigenvalue appears to have an absolute value larger than 15, which is the threshold for 1 fs (in both cases $|\Lambda_1| \approx 19$). On the other hand, in the low temperature case, two eigenvalues appear to have absolute value larger than 15; $|\Lambda_1| \approx 18$ and $|\Lambda_2| \approx 16$. Notice also that in the intermediate and high temperature cases, there is a large gap between the first and the second eigenvalues (i.e., $\Lambda_1 \ll \Lambda_2$). Figure 1 also shows that in all three cases all fast time scales do not change significantly up to ignition, i.e., they retain the same order of magnitude.

Using the TPI diagnostics, the reactions related to the formation of the ultra-fast time scales were identified. In all cases, regardless the initial temperature, the largest TPI of τ_1 (i.e., the system's fastest time scale) was identified to be reaction 1838b ($C_4H_{7(1-3)} + C_2H_3COCH_3 \leftarrow$

$C_8H_{13(1-5,3,TAO)}O$) by 100%. The TPI for the second fastest time scale, i.e τ_2, for the cases that it was determined to be ultra-fast, i.e., when $\tau_2 < 1\ fs$, was identified reaction 893b ($C_3H_2(s) + M \leftarrow C_3H_2 + M$) by 100%. Both findings were consistent with all model fuels, for all tested initial conditions.

Both 1838b and 893b are reverse reactions and no Arrhenius coefficients are provided in the kinetics mechanism. Therefore, their rate constants are calculated based on the related forward and equilibrium constants. Also, 1838b is a unimolecular decomposition reaction, implying that the ultra-fast timescale is a result of an increased reverse rate constant. On the other hand, 893b is an excitation reaction (C_3H_2 is excited to $C_3H_2(s)$) including one reactant plus a "second body", M. Since no efficiency factors are provided for 893b, all species contribute equally as third bodies, thus its reaction rate will be calculated by:

$$R^{893b} = [Mixt] \cdot k_{893b} \cdot [C_3H_2]$$

where $[Mixt]$ stands for the mixture's total concentration and $[C_3H_2]$ represents the concentration of C_3H_2. Considering that $[C_3H_2] << [Mixt]$, it is expected that the maximum value in the elements of the $\boldsymbol{\nabla}(\widehat{\boldsymbol{S}}_{893b}R^{893b})$ matrix will be $[Mixt] \cdot k_{893b}$. Since $[Mixt] \sim \mathcal{O}(10^{-4}) - \mathcal{O}(10^{-3})$ and $|\Lambda_2| \approx 16$ it is reasonable to expect $k_{893b} \sim \mathcal{O}(10^{19}) - \mathcal{O}(10^{20})$. Note that all the rates and orders discussed in CSP analysis are in CGS units.

Table 2 includes the largest rate constants for the three discussed cases at the beginning of each simulation. It is seen that 1838b and 893b are always on the top of this list. Note also that 1838b is the only unimolecular decomposition reaction in the list and that the rate constant value of 893b meets our expectation in the low temperature case (DME/air). Reactions like 2016b and 389f have very large rate constants but they include two reactants each, therefore, their reaction rate gradients (i.e., $\boldsymbol{\nabla}(\widehat{\boldsymbol{S}}_i R^i)$) are significantly decreased. As a result, they do not contribute to the generation of any ultra-fast timescales.

Table 2: The largest rate constants for the 3 discussed cases at $t = 0$. With red are the reactions identified by the TPI diagnostics to relate the most to the system's ultra-fast time scales.

CH_3OCH_3/air		CH_4/air		iC_4H_8/air	
893b	3.76E+19	1838b	3.51E+19	1838b	1.02E+19
2016b	7.57E+18	389f	5.37E+16	389f	1.26E+17
1838b	2.16E+18	1832b	3.84E+16	893b	7.11E+16
389f	3.99E+17	6f	1.18E+16	6f	2.89E+16
6f	9.72E+16	893b	5.18E+15	8f	4.29E+15
1830b	2.07E+16	1484f	3.75E+15	1405b	2.12E+15
2600b	1.59E+16	8f	2.73E+15	1369b	1.61E+15
882b	1.05E+16	1369b	1.77E+15	1484f	1.10E+15
⋮	⋮	⋮	⋮	⋮	⋮
893f	1.00E+13	1838f	1.31E+09	1838f	2.47E+08
⋮	⋮				
1838f	5.28E+06				

Note also that the rate constants of 893f and 1838f in Table 2 are low. In addition, as Table 3 shows, the equilibrium constants of 1838 and 893 reactions are not among the smallest ones.

Thus, by reviewing solely the Arrhenius coefficients provided in the chemical kinetics mechanism and the equilibrium constants, it would be impossible to conclude that reactions 893b and 1838b may relate to ultra-fast timescales. On the other hand, the flaws in 893b and 1838b may be identified by reviewing the rate constants of both forward and backward reactions and taking into account the unimolecular decomposition or isomerization reactions.

Table 3: The reactions with the smallest equilibrium constants for the 3 discussed cases at t=0. With red are the reactions identified by the TPI diagnostics to relate the most to the system's ultra-fast time scales.

CH_3OCH_3/air		CH_4/air		iC_4H_8/air	
1724	1.03E-17	1594	8.68E-17	1594	1.55E-23
2339	1.08E-17	1	2.39E-13	2564	1.41E-21
1689	1.09E-17	662	8.07E-13	1	7.41E-21
2385	1.10E-17	2152	9.36E-13	662	1.14E-20
2377	1.13E-17	1403	1.05E-12	1403	1.24E-20
2334	1.35E-17	2151	4.89E-12	2152	1.57E-20
1180	1.57E-17	2564	9.51E-12	2151	3.22E-19
⋮	⋮	⋮	⋮	⋮	⋮
1838	2.45E-12	1838	3.74E-11	1838	2.41E-11
⋮	⋮				
893	2.66E-07				

In summary, the timescale analysis of the Aramco 2.0 mechanism revealed the following:

- The development of the ultra-fast time scales were independent of the initial pressure, the stoichiometry and the mixture composition (i.e, the fuel), while notable dependence on the initial temperature was observed.
- An ultra-fast timescale ($|\Lambda_1| \approx 18 - 19$) was identified in all examined cases.
- A second ultra-fast timescale ($|\Lambda_2| \approx 16$) was identified at low initial temperatures.
- The TPI diagnostic identified reaction 1838b ($C_4H_{7(1-3)} + C_2H_3COCH_3 \leftarrow C_8H_{13(1-5,3,TA)}O$) to be exclusively related to Λ_1 and 893b ($C_3H_2(s) + M \leftarrow C_3H_2 + M$) to Λ_2. 1838b is a unimolecular decomposition reaction while 893b is an excitation reaction, with all species efficiencies equal to 1.
- The rate constants of 1838b and 893b are calculated based on their related forward and equilibrium constants (i.e., no Arrhenius coefficients are provided for them).
- The rate constants of 1838b and 893b were among the largest ones. In fact, no other unimolecular decomposition/isomerization reaction was found in the list of the ten largest ones.

3.2.2 Ultra-fast timescale analysis of other kinetics models

A similar analysis of ultra-fast timescales was conducted for several other large chemical kinetic models for biodiesel[57], tetrahydropyran[58], and gasoline surrogates[59]. For brevity, the results and discussion for these analyses are provided in the Supplementary Material. In summary, we found that ultra-fast timescales were present in all the kinetic models that we tested. The gasoline surrogates kinetic model[59] was developed at KAUST and exemplifies the need for kinetic modelers to have access to timescale analysis tools during model development.

3.2.3 Impact on computational cost

The existence of ultra-fast timescales has a significant impact on the computational cost, especially when the reaction source terms are integrated explicitly. To demonstrate this effect, 0D and 1D ignition studies of a DME/air and CH_4/air mixtures, respectively, were performed using both explicit and implicit solvers.

The KAUST Adaptive Reacting Flow Solver (KARFS) was employed for all the simulations shown in this section. KARFS is a high-fidelity code for direct numerical simulations of combustion, which solves the fully compressible Navier-Stokes, species and energy equations[60]. The major advantages of KARFS against other CFD codes are its performance-portable capabilities for multi- and many-core heterogeneous platforms. In addition, the employed Kokkos framework[61] allows KARFS to utilize the same source code on CPUs and GPUs while maintaining performance comparable to the code that is optimally tuned to either processing unit[60]. In the following, spatial discretization was carried out by an eighth-order central difference scheme.

To quantify the impact of ultra-fast timescales on the computational cost, in the Aramco 2 mechanism, reaction 1838b (which was identified to be solely related to the system's ultra-fast timescale in all operating conditions) was eliminated. This truncated mechanism is referred to as the "trimmed model", and the results were compared against the full original model. The comparison was done on the basis of three different integration techniques: (a) explicit fourth-order Runge-Kutta (RK4) scheme with fixed timestep, (b) explicit RK4 with variable timestep, using the proportional-integral-derivative (PID) control theory, and (c) operator splitting method, employing implicit integrator (CVODE) for the chemical kinetics and RK4 for the transport (in the 1D case).

The analysis revealed that in the 0D ignition of DME/air ($T(0) = 1{,}300K$, $p(0) = 50atm$, $\varphi = 1.0$) the average wall clock time per integration timestep was the same between the

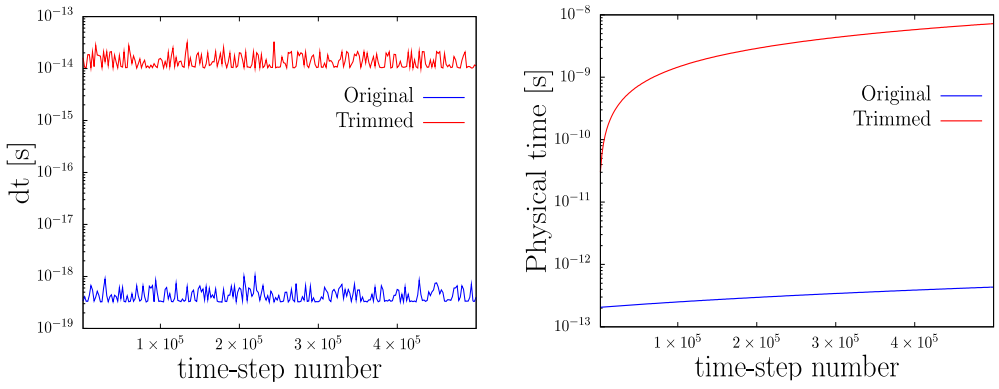

Figure 2: The evolution of dt and the physical time against the number of time-steps for the original and the trimmed Aramco 2 mechanisms during the 0D ignition of DME/air at p(0)=50atm, T(0)=1,300K and φ=1.0. In both cases, the RK4 scheme with variable timestep was utilized. Both simulations run for the same total number of timesteps (500,000).

original and the trimmed models when an implicit solver (CVODE) was used (in both cases the total number of timesteps was set to 5,000). On the other hand, when the RK4 scheme was used with fixed timestep, the trimmed model could be integrated with a timestep $dt = 1 \times 10^{-14}\ s$ but in the case of the original model, the largest possible timestep was $dt = 2 \times 10^{-19}\ s$ for stable time integration. Note that in both cases, the simulations did not reach ignition, since this would require a significant amount of CPU time. Instead, they were run for a sufficiently large number of timesteps (500,000). The difference in the computational cost between the two mechanisms became pronounced when RK4 was used with variable timestep, as shown in Fig. 2. In this case, the average timestep (in the course of 500,000 total timesteps) was $dt \sim \mathcal{O}(10^{-19})\ s$ and $dt \sim \mathcal{O}(10^{-14})\ s$ for the original and the trimmed models, respectively, which correlate perfectly to the system's fastest timescale for each case, as described in the previous subsection. As a result, it becomes obvious that the trimmed model reaches significantly much longer physical time after 500,000 timesteps.

Similar findings were obtained for the 1D ignition problem as well. For both mechanisms, the domain was discretized by a uniform Cartesian grid of 960 points and the domain size was 9.6 mm. The selected mixture was CH_4/air with $p(0) = 1\ atm$ and $\varphi = 1.0$, while temperature was initialized with a gaussian distribution from 800K to 2100K. Finally, both boundaries were modelled as nonreflecting outflows using the Navier-Stokes characteristic boundary conditions (NSCBC)[62]. As observed in the 0D problem, the implicit solver was insensitive to the truncation of the ultra-fast timescale, while a significant impact on the computational time was highlighted when the explicit solver was utilized. In particular, with fixed timestep size, stability of the integration scheme demanded a timestep of $dt = 5 \times 10^{-20}\ s$ in the case of the original mechanism and $dt = 2 \times 10^{-15}\ s$ for the trimmed chemical model. As in the case of 0D ignition, the simulations were run for a sufficiently large number of time steps (~190,000). The results with the variable timestep are shown in Figure 3, where the behavior was found to be consistent with those obtained in the case of fixed timestep. With variable timestep, the average timestep (in the course of 500,000 total timesteps) was $dt \sim \mathcal{O}(10^{-20})\ s$ and $dt \sim \mathcal{O}(10^{-14})\ s$ for the original and the trimmed models, respectively. Consequently, the

original mechanism reaches a significantly smaller physical time compared to the trimmed one in the course of 500,000 timesteps.

The above results clearly demonstrated that the identification and revision of the reactions that generate ultra-fast timescales can have a tremendous impact in the computational time when explicit solvers (with fixed or variable timesteps) are used. As for the implicit time integration schemes, the ultra-fast timescales did not appear to have a significant effect on the computational efficiency. However, the tests were done in a simple 0D and 1D cases, and the CVODE solver based on the backward differentiation scheme is usually robust in following the ignition transient which is the only dominant dynamics of the problem. For a general 3D turbulent combustion simulation in which the relevant physical time scales for turbulent eddies, flames, and acoustic interaction become much shorter, while the physically correct CLC-met

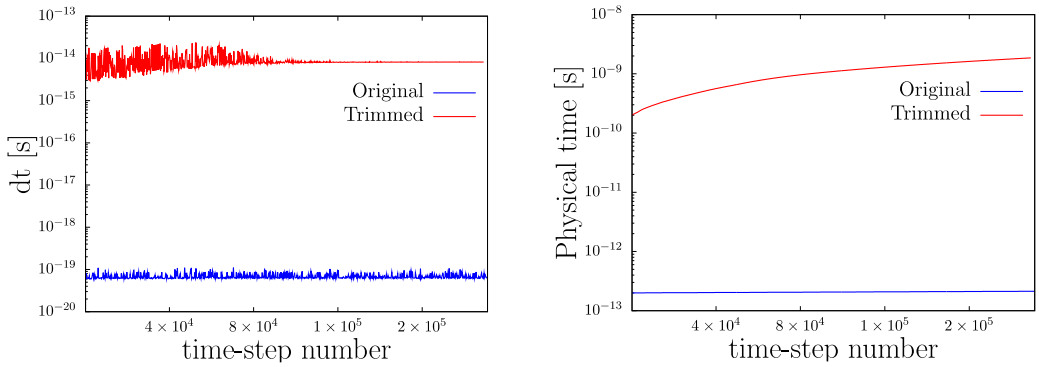

Figure 3: The evolution of dt and the physical time against the number of time-steps for the original and the trimmed Aramco 2 mechanisms during the 1D ignition of CH_4/air at p(0)=1atm and φ=1.0. In both cases, the RK4 scheme with variable timestep was utilized. Both simulations run for the same total number of timesteps (~190,000).

reaction mechanisms are limited to the fast time scales at picoseconds or slower, the computational efficiency of the straightforward explicit scheme versus the operator-splitting implicit scheme must be assessed carefully. In any case, the chemical time scales exceeding the collision limit are unphysical and must be avoided in reliable kinetic models.

4. Summary and Conclusions

The present study presented a systematic investigation of CLC and ultra-fast timescales encountered in detailed kinetic models that are widely applied to combustion simulations. Examples of typical scenarios causing such violations were presented and summarized in detail. Key observations are summarized as:

- CLC violations were identified using the tools provided here, and freely available to users on CloudFlame website and GitHub. This facilitates the identification of sources of error and subsequent correction.
- Ultra-fast timescales can develop in mechanisms of any size. However, large scale mechanisms (i.e., including hundreds of species) are more likely to present such features.

- The ultra-fast timescales are usually generated by reverse unimolecular decomposition/isomerization reactions (i.e., with one reactant) with their rate constants being calculated based on the related forward and equilibrium constants. In such cases, the reverse rate constants are among the largest ones, while the forward and the equilibrium constants may have regular values.
- Reactions with rate constants larger than $O(10^{20})$ are likely to generate ultra-fast timescales.

One of the key findings in this study was that ultra-fast timescales commonly appear in large scale mechanisms consisting of a few hundreds of species or more. This is reasonable because in smaller mechanisms, most of the parameters are well documented and experimentally measured. On the other hand, larger mechanisms contain chemical pathways for which little information is known and analogies are often used to estimate rate parameters and thermochemistry. In such cases, the estimated parameters are often modified based on their ability to fit global observables of the system, such as the ignition delay time. Consequently, the model may be able to predict the global quantities better while the many optimized rate constants are more likely to cause unrealistic artifacts at the molecular level, such as timescales faster than 1 fs. In this paper, we took a simple approach of deleting the faulty reactions, but this is not the ideal solution. Rather, reactions related to these ultra-fast timescales should be identified and have their rate constants properly modified to be within realistic timescales.

In today's combustion research community, detailed kinetic models can be quickly developed and tested in software like Chemkin Pro[63], which circumvents the computational stiffness issues by utilizing implicit solvers like CVODE[64]. On the other hand, state-of-the-art high fidelity multi-dimensional simulations use smaller mechanisms in the size of tens of species, which have been significantly reduced from a detailed model and in some cases quasi-steady state assumptions were introduced, for an *a priori* stiffness removal[15,18]. With the advances in the high performance computing at the exascale, along with the acceleration offered by the manycore architecture, such large scale turbulent combustion simulations are starting to employ much larger kinetic mechanisms to predict realistic combustion systems. In particular, the CPU/GPU hybrid architecture offers an opportunity to accelerate the simulations without having to resort to expensive and iterative implicit time integration schemes[60], and in such cases the need for CLC-met reaction mechanisms is more important.

Therefore, there is a growing need in the combustion community that chemical kinetic mechanisms are developed by complying with the fast time scales within physical limits. We suggest that kinetic models be screened for CLC and ultra-fast timescales and erroneous reaction rates be revisited accordingly. The former screening can be easily performed using our CloudFlame website tool. For the latter, from a CFD perspective, we suggest that published kinetic models be accompanied by stiffness measurements or tests with explicit solvers. This could be performed by experts in the field using specific analytical tools such as CSP.

5. Acknowledgments

This work was supported by the Clean Combustion Research Center at the King Abdullah University of Science and Technology (KAUST).

6. References:

[1] Kohse-Höinghaus K. Clean combustion: Chemistry and diagnostics for a systems approach in transportation and energy conversion. *Prog. Energy Combust. Sci.* 2018;65:1–5.

[2] Sarathy SM, Oßwald P, Hansen N, Kohse-Höinghaus K. Alcohol combustion chemistry. *Prog. Energy Combust. Sci*. 2014;44:40–102.

[3] Mehl M, Pitz WJ, Westbrook CK, Curran HJ. Kinetic modeling of gasoline surrogate components and mixtures under engine conditions. *Proc. Combust. Inst.* 2011;33:193–200.

[4] Sarathy SM, Westbrook CK, Mehl M, Pitz WJ, Togbe C, Dagaut P, Wang H, Oehlschlaeger MA, Niemann U, Seshadri K, Veloo PS, Ji C, Egolfopoulos FN, Lu T. Comprehensive chemical kinetic modeling of the oxidation of 2-methylalkanes from C7 to C20. *Combust. Flame.* 2011;158:2338–2357.

[5] Benson SW. Thermochemical Kinetics. 2nd ed., Wiley, New York, 1976.

[6] Tee LS, Gotoh S, Stewart WE. Molecular Parameters for Normal Fluids. Lennard-Jones 12-6 Potential. *Ind. Eng. Chem. Fundam.* 1966;5:356–363.

[7] Hoff JHV. Etudes de dynamique chimique. Muller, 1884.

[8] Arrhenius S. Über die Reaktionsgeschwindigkeit bei der Inversion von Rohrzucker durch Säuren. *Zeitschrift für Phys. Chemie.* 1889;4:226-248.

[9] Trautz M. Das Gesetz der Reaktionsgeschwindigkeit und der Gleichgewichte in Gasen. Bestätigung der Additivität von Cv-3/2R. Neue Bestimmung der Integrationskonstanten und der Moleküldurchmesser. *Zeitschrift Für Anorg. Und Allg. Chemie.* 2018;96:1–28.

[10] Chen D, Wang K, Wang H. Violation of collision limit in recently published reaction models. *Combust. Flame.* 2017;186:208–210.

[11] Zewail AH. Femtochemistry: Atomic-scale dynamics of the chemical bond using ultrafast lasers (Nobel Lecture). *Angew. Chem.* 2000;39:2586-2631.

[12] Goteng GL, Nettyam N, Sarathy SM. CloudFlame: Cyberinfrastructure for Combustion Research, in: *2013 Int. Conf. Inf. Sci. Cloud Comput. Companion* 2013:294–299. doi:10.1109/ISCC-C.2013.57.

[13] Lam SH, Goussis DA. The CSP method for simplifying kinetics. *Int. J. Chem. Kinet.* 2004;26:461–486.

[14] Lam SH, Goussis DA. Understanding complex chemical kinetics with computational singular perturbation. *Symp. Combust.* 1989;22:931–941.

[15] Massias A, Diamantis D, Mastorakos E, Goussis DA. An algorithm for the construction of global reduced mechanisms with CSP data. *Combust. Flame.* 1999;117:685–708.

[16] Koniavitis P, Rigopoulos S, Jones WP. Reduction of a detailed chemical mechanism for a kerosene surrogate via RCCE-CSP. *Combust. Flame.* 2018;194:85–106.

[17] Prager J, Najm HN, Valorani M, Goussis DA. Skeletal mechanism generation with CSP and validation for premixed n-heptane flames. *Proc. Combust. Inst.* 2009;32:509–517.

[18] Tingas E-A, Diamantis DJ, Goussis DA. Issues arising in the construction of QSSA mechanisms: the case of reduced n-heptane/air models for premixed flames. *Combust. Theory Model.* 2018;22:1049-1083.

[19] Li Y, Alfazazi A, Mohan B, Tingas EA, Badra J, Im HG, Sarathy SM. Development of a reduced four-component (toluene/n-heptane/iso-octane/ethanol) gasoline surrogate model. *Fuel* 2019;247:164-178.
[20] Tingas EA, Kyritsis DC, Goussis DA. Autoignition dynamics of DME/air and EtOH/air homogeneous mixtures. *Combust. Flame.* 2015;162:3263–3276.
[21] Manias DM, Tingas EA, Frouzakis CE, Boulouchos K, Goussis DA. The mechanism by which CH2O and H2O2 additives affect the autoignition of CH4/air mixtures. *Combust. Flame.* 2016;164:111–125.
[22] Manias DM, Tingas EA, Hernandez-Pérez FA, Im HG, Galassi RM, Ciottoli PP, Valorani M. *AIAA Aerosp. Sci. Meet.* 2018:p.364.
[23] Song W, Tingas EA, Im HG. A computational analysis of methanol autoignition enhancement by dimethyl ether addition in a counterflow mixing layer. *Combust. Flame.* 2018;195:84–98.
[24] Jaasim M, Tingas EA, Hernández Pérez FA, Im HG. Computational singular perturbation analysis of super-knock in SI engines. *Fuel.* 2018;225:184–191.
[25] Tingas EA, Manias DM, Mani Sarathy SM, Goussis DA. CH4/air homogeneous autoignition: A comparison of two chemical kinetics mechanisms. *Fuel.* 2018;223:74–85.
[26] Manias DM, Tingas EA, Hernández Pérez FA, Malpica Galassi R, Paolo Ciottoli P, Valorani M, Im HG. Investigation of the turbulent flame structure and topology at different Karlovitz numbers using the tangential stretching rate index. *Combust. Flame.* 2019;200:155–167.
[27] Manias DM, Tingas EA, Minamoto Y, Im HG. Topological and chemical characteristics of turbulent flames at MILD conditions. *Combust. Flame.* 2019;208:86-98.
[28] Tingas EA, Im HG, Kyritsis DC, Goussis DA. The use of CO2 as an additive for ignition delay and pollutant control in CH4/air autoignition. *Fuel.* 2018;211:898–905.
[29] Tingas EA, Wang Z, Sarathy SM, Im HG, Goussis DA. Chemical kinetic insights into the ignition dynamics of n-hexane. *Combust. Flame.* 2018;188:28–40.
[30] Tingas EA, Kyritsis DC, Goussis DA. Comparative investigation of homogeneous autoignition of DME/air and EtOH/air mixtures at low initial temperatures. *Combust. Theory Model.* 2017;21:93–119.
[31] Sarathy SM, Tingas EA, Nasir EF, Detogni A, Wang Z, Farooq A, Im HG. Three-stage heat release in n-heptane auto-ignition. *Proc. Combust. Inst.* 2019;37(1):485-492.
[32] Tingas EA, Kyritsis DC, Goussis DA. Algorithmic determination of the mechanism through which H2O-dilution affects autoignition dynamics and NO formation in CH4/air mixtures. *Fuel.* 2016;183:90–98.
[33] Goodwin DG, Moffat HK, Speth R. Cantera: An Object-oriented Software Toolkit for Chemical Kinetics, Thermodynamics, and Transport Processes. Version 2.2.0, 2015. doi:10.5281/zenodo.48735.
[34] Neufeld PD, Janzen AR, Aziz RA. Empirical equations to calculate 16 of the transport collision integrals Ω(l,8)* for the lennard-jones (12-6) potential. *J. Chem. Phys.* 1972;57:1100-1102.
[35] Zagaris A, Kaper H, Kaper T. Fast and Slow Dynamics for the Computational Singular Perturbation Method. *Multiscale Model. Simul.* 2004;2:613–638.
[36] Lam SH, Goussis DA. Conventional asymptotics and computational singular perturbation for simplified kinetics modelling, in: M.O. Smooke (Ed.), Reduced Kinetic Mechanisms and Asymptotic Approximations for Methane-Air Flames. *Springer Lecture Notes, vol. 384, Springer Verlag*, Berlin, 1991:p. 227.
[37] Valorani M, Goussis DA, Creta F, Najm HN. Higher order corrections in the approximation of low-dimensional manifolds and the construction of simplified

problems with the CSP method. *J. Comput. Phys.* 2005;209:754–786.
[38] Tingas EA, Kyritsis DC, Goussis DA. Ignition delay control of DME/air and EtOH/air homogeneous autoignition with the use of various additives. *Fuel.* 2016;169:15–24.
[39] Manias DM, Diamantis DJ, Goussis DA. Algorithmic Identification of the Reactions Related to the Initial Development of the Time Scale That Characterizes CH4/Air Autoignition. *J. Energy Eng.* 2015;141:4014–15.
[40] Diamantis DJ, Mastorakos E, Goussis DA. H2/air autoignition: The nature and interaction of the developing explosive modes. *Combust. Theory Model.* 2015;19:382–433.
[41] Goussis D, Najm H. Model Reduction and Physical Understanding of Slowly Oscillating Processes: The Circadian Cycle. *Multiscale Model. Simul.* 2006;5:1297–1332.
[42] Kooshkbaghi M, Frouzakis CE, Boulouchos K, Karlin IV. n-Heptane/air combustion in perfectly stirred reactors: Dynamics, bifurcations and dominant reactions at critical conditions. *Combust. Flame.* 2015;162:3166–3179.
[43] Singh E, Tingas EA, Goussis D, Im HG, Sarathy SM. Chemical Ignition Characteristics of Ethanol Blending with Primary Reference Fuels. *Energy & Fuels* 2019; 33(10):10185-10196.
[44] Metcalfe WK, Burke SM, Ahmed SS, Curran HJ. A Hierarchical and Comparative Kinetic Modeling Study of C1 − C2 Hydrocarbon and Oxygenated Fuels. I*nt. J. Chem. Kinet.* 2013;45:638–675.
[45] Zhou CW, Li Y, O'Connor E, Somers KP, Thion S, Keesee C, Mathieu O, Petersen EL, DeVerter TA, Oehlschlaeger MA, Kukkadapu G, Sung CJ, Alrefae M, Khaled F, Farooq A, Dirrenberger P, Glaude PA, Battin-Leclerc F, Santner J, Ju Y, Held T, Haas Fm, Dryer FL, Curran HJ. A comprehensive experimental and modeling study of isobutene oxidation. *Combust. Flame.* 2016;167:353–379.
[46] Li Y, Zhou CW, Somers KP, Zhang K, Curran HJ. The oxidation of 2-butene: A high pressure ignition delay, kinetic modeling study and reactivity comparison with isobutene and 1-butene. *Proc. Combust. Inst.* 2017;36:403–411.
[47] Zhou CW, Li Y, Burke U, Banyon C, Somers KP, Ding S, Khan S, Hargis JW, Sikes T, Mathieu O, Petersen EL, AlAbbad M, Farooq A, Pan Y, Zhang Y, Huang Z, Lopez J, Loparo Z, Vasu SS, Curran HJ. An experimental and chemical kinetic modeling study of 1,3-butadiene combustion: Ignition delay time and laminar flame speed measurements. *Combust. Flame.* 2018;197:423–438.
[48] Smith GP, Tao Y, Wang H. Foundational Fuel Chemistry Model Version 1.0 (FFCM-1), http://nanoenergy.stanford.edu/ffcm1, 2016.
[49] Atef N, Kukkadapu G, Mohamed SY, AlRashidi M, Banyon C, Mehl M, Heufer KA, Nasir EF, Alfazazi A, Das AK, Westbrook CK, Pitz WJ, Lu T, Farooq A, Sung CJ, Curran HJ, Sarathy SM. A comprehensive iso-octane combustion model with improved thermochemistry and chemical kinetics. *Combust. Flame* 2017;178:111–134.
[50] AlRashidi MJ, Mehl M, Pitz WJ, Mohamed S, Sarathy SM. Cyclopentane combustion chemistry. PartI: mechanism development and computational kinetics. *Combust. Flame* 2017;183:358–371.
[51] Mohamed SY, Cai L, Khaled F, Banyon C, Wang Z, AlRashidi MJ, Pitsch H, Curran HJ, Farooq A, Sarathy SM. Modeling ignition of a heptane isomer: improved thermodynamics, reactionpathways, kinetics, and rate rule optimizations for 2-methylhexane. *J. Phys. Chem. A* 2016;120:2201–2217.
[52] Kathrotia T, Riedel U, Seipel A, Moshammer K, Brockhinke A. Experimental and numerical study of chemiluminescent species in low-pressure flames. *Appl. Phys. B Lasers Opt.* 2012;107:571–584.
[53] Tamura M, Berg PA, Harrington JE, Luque J, Jeffries JB, Smith GP, Crosley DR,

Collisional quenching of CH(A), OH(A), and NO(A) in low pressure hydrocarbon flames. *Combust. Flame.* 1998;114:502–514.
[54] Harding LB, Georgievskii Y, Klippenstein SJ. Predictive Theory for Hydrogen Atom−Hydrocarbon Radical Association Kinetics. *J. Phys. Chem. A.* 2005;109:4646–4656.
[55] CSPTk - A Software Toolkit for the CSP and TSR Analysis of Kinetic Models and the Simplification and Reduction of Chemical Kinetics Mechanisms. The software can be obtained upon request to M.Valorani (mauro.valorani@uniroma1.it), (2015).
[56] Safta C, Najm H, Knio O. TChem-A software toolkit for the analysis of complex kinetic models, Sandia Report SAND2011-3282.
[57] Herbinet O, Pitz WJ, Westbrook CK. Detailed chemical kinetic mechanism for the oxidation of biodiesel fuels blend surrogate. *Combust. Flame.* 2010;157:893–908.
[58] Tran LS, De Bruycker R, Carstensen HH, Glaude PA, Monge F, Alzueta MU, Martin RC, Battin-Leclerc F, Van Geem KM, Marin GB. Pyrolysis and combustion chemistry of tetrahydropyran: Experimental and modeling study. *Combust. Flame.* 2015;162:4283–4303.
[59] Sarathy SM, Kukkadapu G, Mehl M, Javed T, Ahmed A, Naser N, Tekawade A, Kosiba G, AlAbbad M, Singh E, Park S, Al Rashidi M, Chung SH, Roberts WL, Oehlschlaeger MA, Sung CJ, Farooq A. Compositional effects on the ignition of FACE gasolines. *Combust. Flame.* 2016;169:171–193.
[60] Hernández Pérez FE, Mukhadiyev N, Xu X, Sow A, Lee BJ, Sankaran R, Im HG. Direct numerical simulations of reacting flows with detailed chemistry using many-core/GPU acceleration. *Comput. Fluids.* 2018;173:73–79.
[61] Carter Edwards H, Trott CR, Sunderland D. Kokkos: Enabling manycore performance portability through polymorphic memory access patterns. *J. Parallel Distrib. Comput.* 2014;74:3202–3216.
[62] Yoo CS, Im HG. Characteristic boundary conditions for simulations of compressible reacting flows with multi-dimensional, viscous and reaction effects. *Combust. Theory Model.* 2007;11:259–286.
[63] CHEMKIN-PRO R. 15112, Reaction Design. Inc., San Diego, CA. 2011.
[64] Cohen SD, Hindmarsh AC, Dubois PF. CVODE, A Stiff/Nonstiff ODE Solver in C, Comput. Phys. 1996;10:138–143.

List of Tables:

List of Figures:

K, φ=2.0) on the left, iC4H8/air (p(0)=30.0 atm, T(0)=1,100 K, φ=1.0) in the middle and CH4/air (p(0)=4.1 atm, T(0)=1,724 K, φ=0.1) on the right.

Figure 2 - The evolution of dt and the physical time against the number of time-steps for the original and the trimmed Aramco 2 mechanisms during the 0D ignition of DME/air at p(0)=50atm, T(0)=1,300K and φ=1.0. In both cases, the RK4 scheme with variable timestep was utilized. Both simulations run for the same total number of timesteps (500,000).

Figure 3 - The evolution of dt and the physical time against the number of time-steps for the original and the trimmed Aramco 2 mechanisms during the 1D ignition of CH4/air at p(0)=1atm and φ=1.0. In both cases, the RK4 scheme with variable timestep was utilized. Both simulations run for the same total number of timesteps (~190,000).